CHEMICAL ENGINEERING TRANSACTIONS
VOL. 117, 2025
A publication of AIDIC
The Italian Association of Chemical Engineering
Online at www.cetjournal.it
Guest Editors: Fabrizio Bezzo, Flavio Manenti, Gabriele Pannocchia, Almerinda di Benedetto

ISBN 979-12-81206-17-5; **ISSN** 2283-9216
DOI: 10.3303/CET25117151

Optimizing Surface Area of Structured Packing via Advanced 3D Printing Techniques

Stefano G. Acierno, Domenico Flagiello*, Daniele Tammaro, Alessandro Erto, Pier L. Maffettone, Amedeo Lancia, Francesco Di Natale

Department of Chemical, Materials and Production Engineering – University of Naples Federico II - P.le Tecchio 80, 80125, Naples, Italy
domenico.flagiello@unina.it

This study focuses on the production of single rectangular sheets, representing the repetitive unit of a structured packing but simplified to a flat geometry without holes or corrugations and explores the use of 3D foam-printing to improve their texture and enhance their surface area and wettability properties for packed column applications. Two types of surface textures (wavy and pyramid patterns) inspired by industrial designs are produced: one set with conventional Polylactic Acid (PLA) filaments and another using CO_2-foamed PLA filaments. The printing and foaming parameters are optimized to maximize the surface area of the textures. Surface properties are analyzed using Scanning Electron Microscopy (SEM) for micro-roughness and confocal microscopy for the full range of roughness. Results show a 5–23% increase in surface area, supporting a more efficient mass transfer. This approach presents a promising pathway for developing advanced, high-performance surfaces for process intensification in packed column applications.

1. Introduction

Gas-liquid contactors are of great interest in chemical engineering, when enhanced mass transfer rates are needed, e.g. in distillation, absorption and stripping. Recently, 3D printing integrated to foaming process has been successfully used to produce structured packing modules for gas absorption (Flagiello et al., 2022, 2023) with a promising enhancement in mass transfer rates. This method combines additive manufacturing with the formation of microcellular foams, resulting in high porosity and intra-strand micropores, thereby altering the overall surface structure. This work aims to understand the role exerted by foam-printing in the fruitful modification of the texture of the packing surface, so to increase surface area. To this end, single rectangular sheets, representing the repetitive unit of a structured packing, were produced using 3D printing technology with PLA filaments. The elements were printed using textured surface patterns of commercial use such as wavy and pyramid designs. Printing and foaming parameters were systematically optimized through iterative processes to maximize the surface area. Advanced optical techniques were used to characterize the samples: scanning electron microscopy (SEM) assessed the micro-roughness induced by foaming, while confocal microscopy analyzed the combined effects of texture and foaming on surface roughness.

2. Materials and methods

2.1 Materials

Polylactic acid (PLA) NW4043D (Nature Works LLC) was used for filament fabrication, with physical properties and processing conditions detailed in Tammaro et al., 2021: PLA pellets were dried overnight at 60°C under vacuum and a 1.75 mm PLA filament was produced using a Composer350 extruder (3DEVO, Netherlands). Carbon dioxide (CO_2) from AirCos (Italy) served as blowing agent for the foaming process.

Paper Received: 7 December 2024; Revised: 22 March 2025; Accepted: 1 May 2025
Please cite this article as: Acierno S.G., Flagiello D., Tammaro D., Erto A., Maffettone P.L., Lancia A., Di Natale F., 2025, Optimizing Surface Area of Structured Packing via Advanced 3D Printing Techniques, Chemical Engineering Transactions, 117, 901-906 DOI:10.3303/CET25117151

2.2 3D printing and foaming set-up

The 3D CAD models of the sheet samples were designed in Fusion Autodesk 360® and printed with a Prusa I3 MK3S FFF 3D printer. This printer has a heated bed, a single extruder, automatic bed levelling and a filament sensor for reliability and ease of use. More details on the printer are available in Galati et al., 2019. CO_2 was solubilized into the PLA filament as a blowing agent using a high-pressure autoclave, operated at room temperature and 50 bar to prevent thermal effects on the agent's behavior. The pretreatment followed the protocol outlined by Tammaro et al. (2021), ensuring precise control over the foaming process.

2.3 Optimization procedure for 3D printing and 3D foam printing

Printing and foaming parameters were iteratively optimized to maximize surface area, using a smooth sheet as reference. This simplified approach was chosen because cell size distribution principles are expected to remain consistent across textured and un-textured sheets, making the optimized parameters potentially transferable to more complex geometries. To ensure high surface quality and structural integrity, the printing parameters were optimized for the production of smooth (un-foamed) PLA sheets. A nozzle diameter (D_{nozzle}) of 0.6 mm and a layer height (δ_{layer}) of 0.2 mm were chosen to balance textural precision and geometric accuracy. The print speed (u_{print}) was set at 80 mm/s for efficient printing without compromising quality. Filament flow rate (Q_f) and infill density (ρ_{infill}) were maintained at 95% and 100%, respectively, for mechanical strength. The build plate temperature (T_{plate}) was kept at 60°C, above the glass transition temperature of PLA, to stabilize the process, while raster angle (0-90°) and nozzle temperature (190-260°C) were investigated as independent variables. The optimization was conducted by analyzing only the extremes of the ranges for both parameters. Initially, the influence of θ_{raster} on surface roughness was evaluated with T_{print} fixed at 190°C. Subsequently, once the optimal θ_{raster} value that maximized roughness parameters was determined, the influence of T_{print} was assessed. Once the 3D printing parameters were optimized, the foaming process was refined using CO_2-foamed filaments. T_{foam} (220–250°C) and u_{foam} (60–100 mm/s) were varied, while D_{nozzle}, δ_{layer}, Q_f, ρ_{infill}, T_{plate} and θ_{raster} remained constant. The narrower T_{foam} range accounted for the CO_2 plasticizing effect, which required higher temperatures to avoid filament blockage. The u_{foam} values below 60 mm/s were excluded due to impractical print times, while speeds above 100 mm/s compromised fine textures.

2.4 Optical analysis

The surface roughness of the sheets was analyzed with a Hitachi TM 3000 SEM. Samples were cut with a razor blade in liquid nitrogen, gold-coated by sputtering and examined under SEM, following the method in Flagiello et al., 2022. ImageJ® software was used to estimate cell size (N_{cell} [µm]), Feret diameter was used to determine the characteristic cell size and to calculate the percentage size distribution (PSD) of the cells. Confocal microscopy was also performed to verify uniform surface coverage. The parameters analyzed included: arithmetic mean deviation (R_a [µm]), root mean square deviation (R_q [µm]), skewness (R_{sk}), kurtosis (R_{ku}), maximum peak height (R_p [µm]), maximum valley depth (R_v [µm]), maximum height (R_z [µm]) and the surface complexity S_{dr} [%], defined as the ratio by the actual surface area (A_r [mm²]) to the projected area (A_p [mm²]), which corresponds to the flat, two-dimensional area derived from the sheet dimensions (constant for all samples). However, 3D printing is inherently imprecise and results in a non-zero surface roughness. Thus, the actual surface area (A_r) exceeds the geometric area CAD detected (A_{CAD} [mm²]). To determine (A_r), the projected area (A_p) was first calculated. S_{dr} value was then used to estimate the roughness-induced area increase. For each sample, both foamed and un-foamed, this increment was added to the geometric area (A_{CAD}) to obtain the actual area (A_r). The measured area was then compared to the geometric area to evaluate the effect of surface roughness. Several metrics were calculated to quantify the differences: the percentage increase in area between the actual and geometric areas (AGR, Actual-to-Geometric Ratio), the percentage increase in area of textured samples relative to the smooth sheet benchmark (TSR, Textured-to-Smooth Ratio) and the surface roughness enhancement (S_{enh}) between un-foamed and foamed sheets:

$$AGR = \frac{A_r - A_{CAD}}{A_{CAD}} \tag{1}$$

$$TSR = \frac{A_{r,t} - A_{r,s}}{A_{r,s}} \tag{2}$$

$$S_{enh.} = \frac{A_{r,f} - A_{r,u}}{A_{r,u}} \tag{3}$$

where $A_{r,t}$ is the actual surface area of textured sheet samples, $A_{r,s}$ is referred to the smooth one, while $A_{r,f}$ and $A_{r,u}$ are the actual surface area referred to foamed and un-foamed samples.

3. Results and Discussion

3.1 Optimization procedure for 3D printing

The temperature was fixed at 190 °C, assuming that the effects of θ_{raster} and T_{print} on the roughness are independent. Table 1 lists the roughness metrics R_a, R_q, R_z, R_{sk} and R_{ku} measured by the confocal microscope for the two θ_{raster} investigated (θ_{raster} = 0° and θ_{raster} =90°).

Table 1: Roughness parameters for θ_{raster} = 90° and θ_{raster} = 0°

θ_{raster} [°]	R_a [µm]	R_q [µm]	R_z [µm]	R_{sk} [-]	R_{ku} [-]
90	1.1±0.2	1.3±0.2	5.5±0.6	0.4±0.1	1.1±0.1
0	7.8±0.8	8±1	27± 2	-0.2±0.1	3.7±0.2

The data in Table 1 indicate that surfaces are significantly rougher at θ_{raster} = 0° than at 90°. The R_a value is seven times higher and R_q confirms greater roughness at 0°. R_z further highlights deeper valleys and sharper peaks, particularly at 0°, while R_{sk} values near zero indicate a symmetrical peak-valley distribution for both angles. The increased roughness at 0° is due to the shorter mean deposition length, leading to higher accelerations and more frequent peaks and valleys during printing. Based on these findings, θ_{raster} = 0° was selected as the optimal value for subsequent optimization. Figure 1 shows samples printed at 190°C (a, c) and 260°C (b, d) with θ_{raster} = 0°. Both top-view (a, b) and profile-view (c, d) images illustrate the deposition behavior of the molten filament. Table 2 summarizes the roughness parameters and their standard deviations, measured using a confocal microscope, for both surfaces.

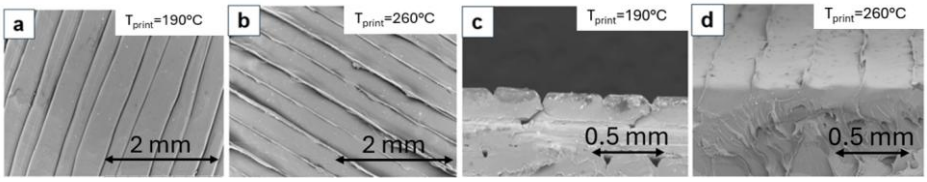

Figure 1: SEM Images. Top view of a portion of the analyzed sample for (a) T_{print} = 190°C and (b) T_{print} = 260°C; cross-sectional view of a segment of the sample surface for (c) T_{print}=190°C and (d) T_{print}= 260°C

Table 2: Roughness parameters for T_{print} = 190°C and T_{print} = 260°C

T_{print} [°C]	R_a [µm]	R_q [µm]	R_z [µm]	R_{sk} [-]	R_{ku} [-]
190	7.8±0.8	8±1	27± 2	-0.2±0.1	3.7±0.2
260	1.2±0.1	1.5±0.1	6.9±0.5	0.2±0.1	3.5±0.4

The data in Table 2 show that the surface printed at 190°C exhibits greater micro-roughness, as indicated by R_a, R_q and R_z values. Figure 1 highlights the effect of temperature on PLA viscosity and its impact on deposition behavior. At 190°C (Figures 1a, 1c), the polymer is extruded discontinuously, forming grooves at layer interfaces. This is further supported by an R_{sk} value below zero, indicating a surface dominated by valleys. Conversely, at 260°C (Figures 1b, 1d), where R_{sk} is greater than zero, no grooves form; instead, excess material accumulates along the sides. This behavior results from the inverse relationship between viscosity and temperature. At lower temperatures, higher viscosity enhances cohesion, leading to void formation and increased roughness. At higher temperatures, reduced viscosity allows the molten PLA to spread more evenly, minimizing air gaps and producing smoother ridges.

3.2 Optimization procedure for 3D foam-printing

Figure 2 shows scanning electron microscope (SEM) micrographs of the foamed sheet surface at different foaming temperatures (220°C to 250°C). Other printing parameters were set as follows: D_{nozzle} = 0.6 mm, δ_{layer} = 0.2 mm, θ_{raster} = 0°, Q_f = 95%, ρ_{infill} = 100%, T_{plate} = 60°C, and u_{foam} = 80 mm/s, maintaining constant flow conditions to isolate the effect of T_{foam} on foaming behavior.

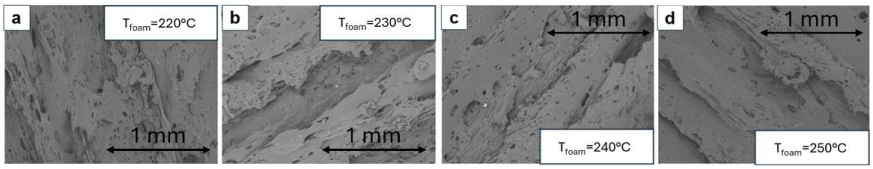

Figure 2: SEM image for T_{foam} optimization. u_{foam} = 80 mm/s: a) 220 °C, b) 230 °C, c) 240 °C and d) 250 °C

The images show how T_{foam} affects cell size and distribution. At 220°C (Figure 2a), cells are small, spherical and tightly packed, indicating minimal foaming. At 230°C (Figure 2b), the cells become larger, more irregular, and show early signs of coalescence with increased porosity. At 240°C (Figure 2c), the cells are significantly larger, highly irregular and show significant coalescence, resulting in the highest porosity and most pronounced foaming. However, at 250°C (Figure 2d), the cells shrink and regain uniformity, indicating structural collapse. These observations highlight that excessive temperature destabilizes the foam, while T_{foam} = 240°C optimizes foaming by maximizing cell size and porosity. The burst cells at 240°C form surface craters that increase micro-roughness and improve the solid-liquid contact angle.
Figure 3a shows the percentage size distribution (PSD) of cells as a function of cell size (N_{cell}) for different T_{foam} values, while Figure 3b shows the weighted average cell size ($N_{cell,m}$) as a function of T_{foam}.

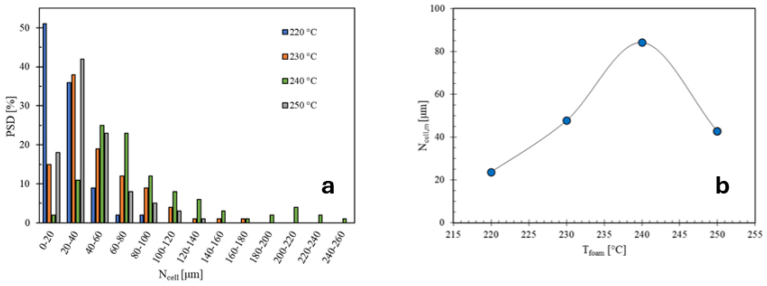

Figure 3: PSD vs N_{cell} at T_{foam} = 220°C/ 230°C/ 240°C/250°C (blue/orange/green/gray) (a). $N_{cell,m}$ as a function of T_{foam} (b) for u_{foam} = 80 mm/s

The cell size has a non-monotonic trend as function of the temperature, with a maximum at 240°C (200-260 µm). At 220°C, nearly 50% of cells are smaller than 40 µm, which is below the typical liquid film thickness in separation processes (100 – 300 µm). By 230°C, the cell size distribution shifts toward larger sizes. Below 240°C, limited heat transfer hinders rapid expansion and crystallization traps CO_2, restricting foaming, while above 240°C, low viscosity accelerates gas escape and matrix collapse. The optimal foaming temperature, T_{foam} = 240°C, was selected to effectively balance these effects, thereby ensuring maximum foaming efficiency. To optimize the foaming speed (u_{foam}), print speed was varied between 60 mm/s and 100 mm/s while maintaining T_{foam} = 240°C. Figure 4 shows SEM micrographs illustrating the impact of these variations on cell formation.

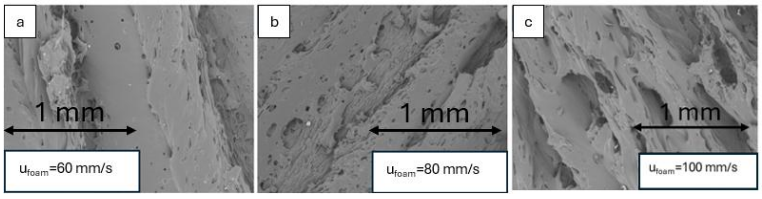

Figure 4: SEM image for u_{foam} optimization. T_{foam} = 240 °C: a) 60 mm/s, b) 80 mm/s and c) 100 mm/s

Cells elongate along the nozzle's motion path. When u_{foam} = 60 mm/s (Figure 4a), cells are relatively small, spherical, and uniformly distributed. The surface appears dense with moderate porosity, indicating that a lower foaming velocity produces smaller cells. For u_{foam} = 80 mm/s (Figure 4b), cells are larger and more irregular in shape. Some cell coalescence is visible, suggesting the merging of smaller cells into larger ones. The surface is noticeably more porous, indicating that increased foaming velocity enhances cell formation and expansion. For u_{foam} = 100 mm/s (Figure 4c), the cells are the largest and most irregular, with significant coalescence, and the surface exhibits the highest porosity and an open structure. The maximum cell size is achieved at u_{foam} = 100 mm/s, which was selected as the optimal foaming speed. Figure 5a shows the percentage size distribution

(PSD) of cells as a function of cells size (N_{cell}) for foamed sheets with T_{foam} = 240°C and varying u_{foam} while in Figure 5b it is reported $N_{cell,m}$ as a function of u_{foam}.

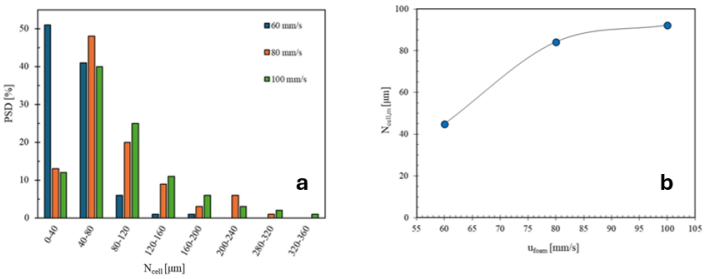

Figure 5: PSD vs N_{cell} for u_{foam} values of 60/80/100 mm/s (blue/orange/green) (a). $N_{cell,m}$ as a function of u_{foam} at T_{foam} = 240°C (b)

Figure 5a shows that N_{cell} increases with print speed, shifting the dominant size range from about 80 µm at 60 mm/s up to 80–120 µm at higher speeds. This growth results from rapid cell depressurization, forming larger bubbles. These findings align with the literature (Tammaro et al., 2016), which links higher speeds to increased pressure drop rates and nucleation rates. Figure 5b indicates that at 100 mm/s, N_{cell} reaches a plateau around 90–95 µm, likely due to temperature non-uniformity in the nozzle (Esposito et al. 2024). This uneven distribution lowers the polymer's average temperature, inhibiting bubble nucleation and growth, a known effect in high-speed 3D printing (Tammaro et al., 2021).

3.3 Production of un-foamed and foamed sheets

The optimized printing procedure was utilized to produce three sheets, both foamed and un-foamed. In addition to a basic smooth sheet, the others featured commercially relevant textured patterns, including wavy and pyramid designs. These patterns had a height of 1 mm, which is comparable to the typical liquid film thickness (0.1–1 mm (Trifonov, 2018, Kapoustina et al., 2015)).

3.4 Optical characterization of sheet samples

For each sheet, Table 3 provides detailed measurements of the increase in the actual surface area, Ar, compared to the projected area, A_p, expressed by the parameter S_{dr} obtained from confocal microscope analysis. Furthermore, it includes the actual area (A_r), the percentage increase between the actual and the geometric areas AGR (Actual-to-Geometric Ratio) and the percentage increase in area TSR (Textured-to-Smooth Ratio), between the different textured samples compared to the smooth sheet, used as benchmark.

Table 3: Un-foamed and foamed sheets area and percentage increase evaluation

	Smooth Un-foamed	Smooth Foamed	Wavy Un-foamed	Wavy Foamed	Pyramidal Un-foamed	Pyramidal Foamed
S_{dr} [%]	3.5 ± 0.2	15 ± 2	24.1 ± 0.8	33 ± 3	23.1 ± 0.6	42 ± 4
A_r [mm²]	3726 ± 7	4170 ± 20	6580 ± 30	6900 ± 20	5580 ± 20	6880 ± 40
AGR [%]	4 ± 0.2	16 ± 2	15 ± 0.5	21 ± 2	18 ± 0.4	45 ± 3
TSR [%]	-	-	77 ± 0.4	66 ± 0.2	50 ± 0.3	65 ± 0.8
$S_{enh.}$ [%]	-	12 ± 1	-	5 ± 0.2	-	23 ± 1

Data in Table 3 highlights the inherent imprecision of 3D printing and that the actual measurements of surface area (A_r) must account for the effect of roughness values, considering S_{dr} parameter. The AGR parameter shows an area increase from 4 to 18% for un-foamed sheets and 16 to 45% for foamed ones. Smooth samples exhibited minimal increases due to the absence of textures. Textured un-foamed sheets showed a similar area increase (15–18%), while for the foamed samples an increase of up to 45% was observed for the pyramidal texture, which was found to be the roughest texture with the foaming process. However, this sheet had a lower Ar (5577 mm²) than the wavy one. At the same time the TSR parameter confirms the benefits of texturing, with area increases up to 76% for the un-foamed wavy sheet and 66% for its foamed version. Interestingly, for the pyramidal sheet, TSR rose from 50% to 65% with foaming, likely due to its greater textured surface, leading to better foaming. Overall, texturing optimizes surface area and foaming amplifies this effect. Notably, the surface area increased significantly, leading to an impressive surface enhancement ($S_{enh.}$) especially for foamed

pyramidal textures (+23% compared to un-foamed samples). Confocal microscopy and chromatic roughness scales (Figure 6) visually depict these surface changes and the impact of foaming on textures.

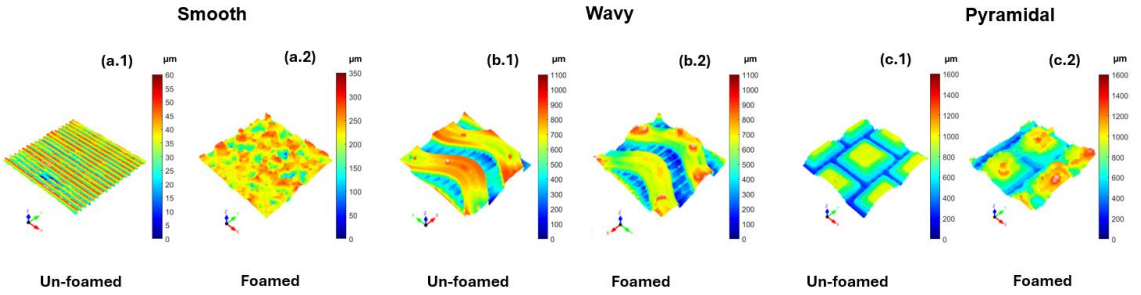

Figure 6: Three-dimensional reconstruction of un-foamed and foamed 3D-printed sheets surface

The analysis of textured sheets revealed notable roughness variations compared to the smooth sheet, influenced by texture shape, depth and surface characteristics. The addition of a foaming agent in the PLA filament significantly modified surface morphology. For the smooth sheet, grooves formed due to the rapid release of CO_2 from the polymer matrix (Figure 6(a.2)), elongating cells in the direction of the printer nozzle and increasing surface area relative to the un-foamed version (Figure 6(a.1)). For wavy textures (Figure 6(b.1-b.2)), the 3D foam-printing process led to only a 5% surface area increase. The complex geometry, with sharp curves and protrusions, hindered uniform foaming agent distribution and gas release, limiting cell growth. Conversely, the pyramidal foamed sheet (Figure 6(c.1-c.2)) exhibited significant surface expansion. Its structure, built with five 0.2 mm layers of decreasing size, required lower PLA flow rates, promoting void formation and enhancing surface area growth.

4. Conclusions

Additive manufacturing for polymer materials, commonly known as 3D printing, has been combined with an environmentally friendly foaming process using CO_2 as a blowing agent to produce textured sheets. These textures serve as the building blocks for structured packings designed to optimize and customize gas-liquid separation processes and packed tower applications. The 3D foam printing parameters were optimized (θ_{raster} = 0°, T_{foam} = 240 °C, and u_{foam} = 100 mm/s) to produce foamed PLA sheets with different textures to maximize surface area. An advanced optical analysis was used for comprehensive surface characterization, revealing a 5% to 23% increase in surface area due to the foaming process. This study demonstrates that 3D printing, especially when combined with surface foaming techniques, is an effective approach for developing advanced gas-liquid contactors.

References

Esposito C., Tammaro D., Posabella P., Villone MM., D'Avino G., Maffettone P.L., 2024, Orientation-Graded Morphologies in Microcellular Foams through Additive Manufacturing, Industrial & Engineering Chemistry Research, 63, 42.

Flagiello D., Tammaro D., Erto A., Maffettone P.L. , Lancia A., Di Natale F., 2022, Foamed structured packing for mass-transfer equipment produced by an innovative 3D printing technology, Chem Eng Sci, 260.

Flagiello D., Tammaro D., Erto A., Maffettone P.L., Lancia A., Di Natale F., 2023, Performances of a Y-type structured packing produced by 3D foam-printing for the intensification of gas absorption processes, Chemical Engineering Research and Design,195, 637–650.

Tammaro D., Della Gatta R., Villone M.M., Maffettone P.L., 2021, Continuous 3D Printing of Hierarchically Structured Microfoamed Objects, Adv Eng Mater, 24, 5.

Tammaro D., Astarita A., Di Maio E., Iannace S., 2016, Polystyrene Foaming at High Pressure Drop Rates, Ind Eng Chem Res, 55, 5696–5701.

Galati M., Minetola P., Marchiandia G., Atzenia E., Calignanoa F., Salmia A., Iuliano L., 2019, A methodology for evaluating the aesthetic quality of 3D printed parts, Procedia CIRP, 79, 95–100.

Kapoustina V., Ross-Jones J., Hitschler M., Rädle M., Repke J.U., 2015, Direct spatiotemporally resolved fluorescence investigations of gas absorption and desorption in liquid film flows, Chemical Engineering Research and Design, 99, 248–255.

Trifonov Y.Y., 2011, Counter-current gas-liquid flow between vertical corrugated plates, Chem Eng Sci, 66, 4851–4866.